Rotational Maneuver of Ferromagnetic Nanowires for Cell Manipulation

Yi Zhao*, *Member, IEEE*, and Hansong Zeng

***Abstract*—1-D magnetic nanowires provide a powerful tool for investigating biological systems because such nanomaterials possess unique magnetic properties, which allow effective manipulation of cellular and subcellular objects. In this study, we report the rotational maneuver of ferromagnetic nanowires and their applications in cell manipulation. The rotational maneuver is studied under two different suspension conditions. The rotation of nanowires in the fluid is analyzed using Stokes flow assumption. Experimental results show that when the nanowires develop contacts with the bottom surfaces, the rotational maneuver under a modest external magnetic field can generate rapid lateral motion. The floating nanowires, on the other hand, do not exhibit substantial lateral displacements. Cell manipulation using skeletal myoblasts C2C12 shows that living cells can be manipulated efficiently on the bottom surface by the rotational maneuver of the attached nanowires. We also demonstrate the use of rotational maneuver of nanowires for creating 3-D nanowire clusters and multicellular clusters. This study is expected to add to the knowledge of nanowire-based cell manipulation and contribute to a full spectrum of control strategies for efficient use of nanowires for micro-total-analysis. It may also facilitate mechanobiological studies at cellular level, and provide useful insights for development of 3-D *in vivo*-like multicellular models for various applications in tissue engineering.**

***Index Terms*—Cell manipulation, ferromagnetic nanowires, tissue engineering.**

I. Introduction

MANIPULATION of living cells is a critical process widely involved in fundamental and applied biomedical applications, especially for cell-based diagnosis [1]. During the past decades, a broad array of noninvasive cell manipulation technologies has been developed, including microfluidic approaches [2], dielectrophoretic approaches [3], [4], optomechanical approaches [5], etc. In particular, magnetic nanoparticles have been proved efficient for cell manipulation, separation, and patterning [6]–[9]. The large surface-to-volume ratio of the nanoparticles allows strong and specific binding with various biological objects [10]. These nanoparticles attached to living cells or being internalized by the cells can be actuated by an external magnetic field for manipulation purposes. Among various forms of nanoparticles, 1-D magnetic nanowires with large aspect ratios have recently drawn extensive interests due to their larger magnetic dipole moments [11]. The characteristic cross-sectional dimensions of these nanowires range from a few tens of nanometers to several hundreds of nanometers, while the length is on the order of a few micrometers and above. Such geometries provide a unique micro/nanointerface to wire nanowires with "bigger" surroundings, important for development of various functional devices [12]. Previous studies have demonstrated that magnetic nanowires are more efficient in cell separation than spherical magnetic nanoparticles [13]. The enhanced magnetic forces can also deform polymer materials and apply mechanical loads on single cell level [14]. Most of current studies concentrate on manipulation of magnetic nanowires within the lateral plane, while little is reported on other forms of motion induced by magnetic nanowires. In this paper, we report the "*rotational maneuver*" of magnetic nanowires under a rotating magnetic field, which is defined as the motion that brings the nanowires out of the lateral plane. Such motion can lead to more efficient lateral displacement than in-plane manipulation. It thus allows rapid manipulation of nanowires or cell–nanowire couples. The study is also useful for building 3-D assemblies of cell–nanowire couples, which may open new perspectives for various biomedical applications.

Manuscript received May 8, 2008; revised February 17, 2009. Current version published January 4, 2010. This work was supported by the Department of Biomedical Engineering, Institute for Materials Research, and Mathematical Bioscience Institute, the Ohio State University. *Asterisk indicates corresponding author.*

*Yi Zhao is with the Laboratory for Biomedical Microsystems, Department of Biomedical Engineering, The Ohio State University, Columbus, OH 43210 USA (e-mail: zhao.178@osu.edu).

H. Zeng is with the Laboratory for Biomedical Microsystems, Department of Biomedical Engineering, The Ohio State University, Columbus, OH 43210 USA.

Color versions of one or more of the figures in this paper are available online at http://ieeexplore.ieee.org.

Digital Object Identifier 10.1109/TNB.2009.2025131

II. Materials and Methods

A. Nanowire Synthesis

The rotational maneuver was demonstrated using nickel nanowires because their unique ferromagnetic properties allow easy manipulation by external magnetic fields. Fig. 1(a) shows the electroplating process for nickel nanowires synthesis. An anodic alumina membrane with controlled pore sizes [see Fig. 1(b)] (Fisher Scientific, Pittsburgh, PA) was used as the template for growing nanowires. GaIn eutectic alloy (Sigma-Aldrich, St. Louis, MO) was applied to one side of the membrane surface as the seed layer. After attaching the membrane to a copper plate, the surface of the copper plate was covered with an electric tape, only exposing the area of the porous alumina membrane. This was to avoid the electrochemical reaction between the copper and the electrolyte. Afterward, the copper plate was electrically connected with a nickel wire and immerged into the nickel plating solution (Ni Pure, Technic, Inc., Cranston, RI). During electroplating, the copper plate carrying the membrane served as the anode and the nickel wire served as the cathode. Nickel was growing in the nanopores of the anodic alumina membrane under a dc electrical bias of 1.5 V.

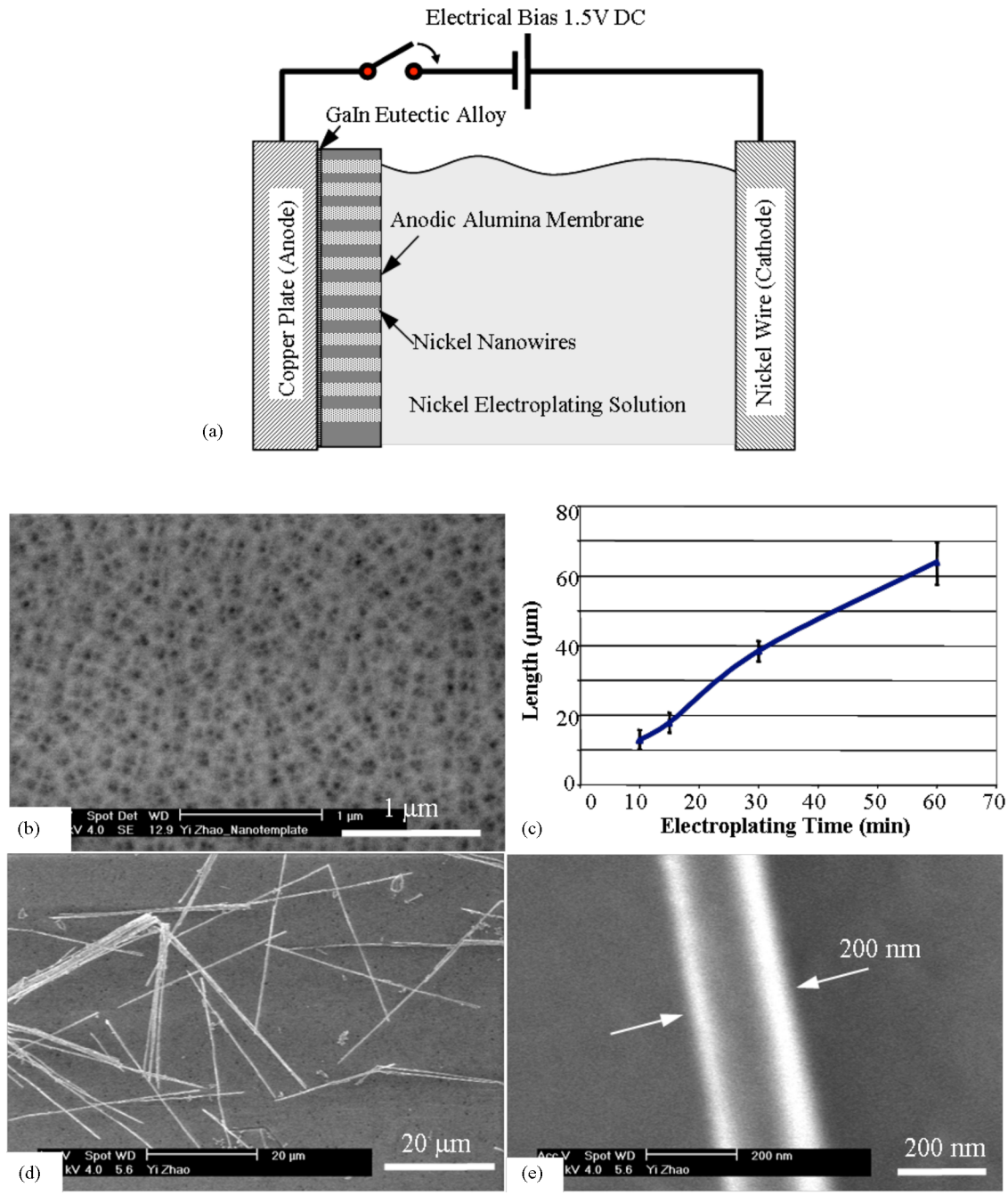

Fig. 1. Nickel nanowires were synthesized by electroplating on a porous alumina anodic membrane. (a) Electroplating under an electrical bias of 1.5 V dc. (b) Nanowires growing into the pores of the alumina anodic membrane. (c) Length of the nanowires controlled by the electroplating time. (d) and (e) SEM micrographs of the as-fabricated nickel nanowires. The diameter of the nanowires is about 200 nm.

The diameter of the nanowires was determined by the pore size of the anodic alumina membrane. The length of the nanowires was controlled by the electroplating time [see Fig. 1(c)]. To demonstrate the efficacy of the rotational maneuver, nanowires with lengths ranging from 10 to 60 μm were synthesized. After the completion of the electroplating process, the anodic alumina membrane was detached from the copper plate. GaIn eutectic alloy was removed using concentrated nitric acid. The alumina membrane was dissolved in NaOH solution (20 wt%). The released nanowires were collected and suspended into phosphate buffer solution (PBS). The concentration of the nanowire suspension was determined by optical microscopy. Fig. 1(d) shows the SEM micrographs of the released nanowires. The diameter of the released nanowires was measured as about 200 nm [see Fig. 1(e)].

B. Cell Culture and Incubation with Nanowires

The nanowires were sterilized in ethanol (70 wt%), and precipitated by centrifugation at 900 r/min for 5 min. These nanowires were then resuspended into the culture medium (Dulbecco's modified Eagle medium (DMEM; Invitrogen, CA)

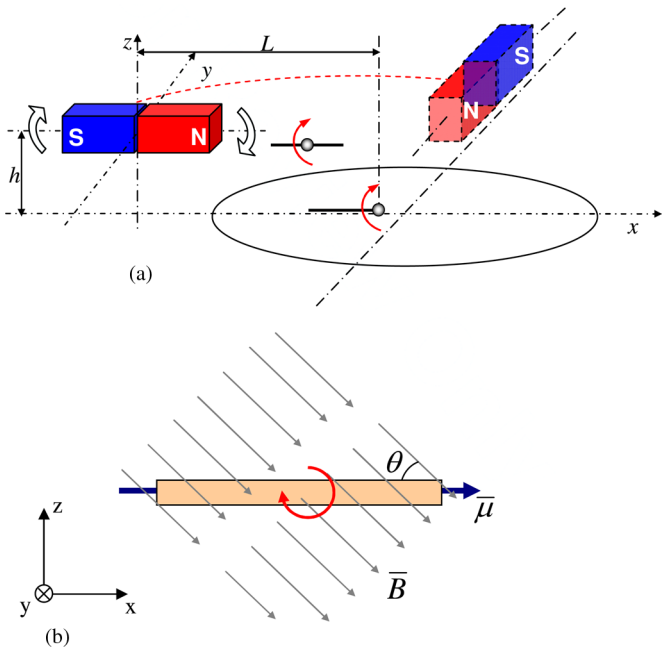

Fig. 2. Rotational maneuver of the nanowires was studied using a rotating external magnetic field. (a) Field generated using permanent magnets positioned close to the point of interest. (b) Interaction between the external field and the induced magnetic dipole moment rotates the nanowire out of the lateral plane.

supplemented with 10% fetal bovine serum, 2 mM glutamine, and 1% penicillin/streptomycin), kept in the incubator at 37 °C, and sonicated for 5 min to avoid aggregation before being mixed with the cells. The nanowires were exposed to the field excess 2000 G. Given the linear relationship between the length of the nanowire and the saturation field strength [13], such a field is sufficient for full remanent magnetization.

Cell manipulation by the rotational maneuver of nanowires was demonstrated using skeletal myoblasts C2C12 (ATCC, MD). The cells were growing in the culture medium according to the protocols described earlier [15]. After the cells proliferated to reach the desired density, they were trypsinized, resuspended in the culture medium and mixed with the PBS containing slightly overnumbered nanowires. The mixture was stirred thoroughly. Optical observation showed that most cells were well attached to one or more nanowires. This is attributed to cell affinity with hydrophilic surfaces of native nickel oxide layer [16]. The disengagement of nanowires from the cell was not observed throughout the entire experiment. The cell–nanowire couples were then aspirated and added to the culture medium in a 100-mm petri dish at 1×10^5 cm^{-2}.

C. Experimental Setup

Fig. 2(a) illustrates the experimental setup for generating rotational maneuver of the nanowires with a rotating magnetic field, where a petri dish containing nanowire suspension was placed on the stage of a measuring microscope. The external magnetic field was generated by a rectangular sintered ceramic ferrite permanent magnet. The magnet is 4.75 cm in length, 2.22 cm in width, and 0.95 cm in thickness. It was positioned on the stage close to the petri dish. The distance from the point of interest to the center of the magnet was about 5.4 cm. The magnet was able to rotate at an arbitrary angle within xz or yz plane along the lateral axis (y-axis or x-axis), respectively. The rotation rate was controllable. The field measurement showed that the magnetic field at the point of interest ranged from about 50 G to about 200 G, depending on the orientation of the magnet. The interaction between the external rotating field and the field-induced magnetic dipole of the nanowire (m) generates a magnetic torque as [11]:

$$M_{\mathrm{DR}} = mlH \sin\theta \tag{1}$$

where l is the length of the nanowire, H is the magnetic field strength, and θ is the lag angle between the driving field and field-induced moment. From this equation, a larger torque can be generated toward a longer nanowire under the same field strength. If such torque was sufficient to rotate the nanowire along the y-axis [driven by the left magnet in Fig. 2(a)], the motions out of the lateral plane will be induced and align the nanowire along the external magnetic field [see Fig. 2(b)]. Similarly, the rotation of the nanowires along x-axis was realized by placing a second permanent magnet perpendicular to the first one [the right magnet in Fig. 2(a)]. The nanowires or cell–nanowire couples can thus rotate along any arbitrary axis in the lateral surface. Under certain suspension conditions, such rotational maneuver is able to induce lateral displacements of the nanowires. Given the fact that the characteristic dimensions of the permanent magnet are orders larger than the dimensions of an individual nanowire, the field gradient within a subject nanowire is very small. The lateral traveling velocity induced by the pull force due to the field nonuniformity is orders lower than that due to the rotating field, and is negligible. By using a rotating external magnetic field, complex fabrication of micromagnets [17] or microshaped metal contacts [18], [19] in the local areas are precluded, easy magnetic manipulation at the small scales is thus allowed.

D. Nanowire Manipulation Using a Rotating Magnetic Field

The rotational maneuver of a nanowire was governed by the driving magnetic torque and the fluidic drag force. For analysis simplicity, it is assumed that the subject nanowire has a constant cross-sectional area along the length, and a homogeneous mass density. Depending on the suspension condition of the nanowire, there are two distinct types of rotational maneuvers. For a nanowire floating in the medium without any contact with the bottom surface, the nanowire rotates around its midpoint under the external field [see Fig. 3(a)]. The fluidic drag resistance torque ($M_{\mathrm{RI\_MID}}$) can be determined by assuming the Stokes flow. According to Bernoulli equation, $M_{\mathrm{RI\_MID}}$ can be determined as

$$M_{\mathrm{RI\_MID}} = \int_{-l/2}^{l/2} \frac{\omega_1^2 x^2 \rho}{2} D\,dx = \frac{\omega_1^2 \rho D l^4}{64} \tag{2}$$

where ρ is the mass density of the medium. The angular rotational velocity (ω_1) at equilibrium can be derived when the fluidic resistance torque in (2) equals to the driving magnetic

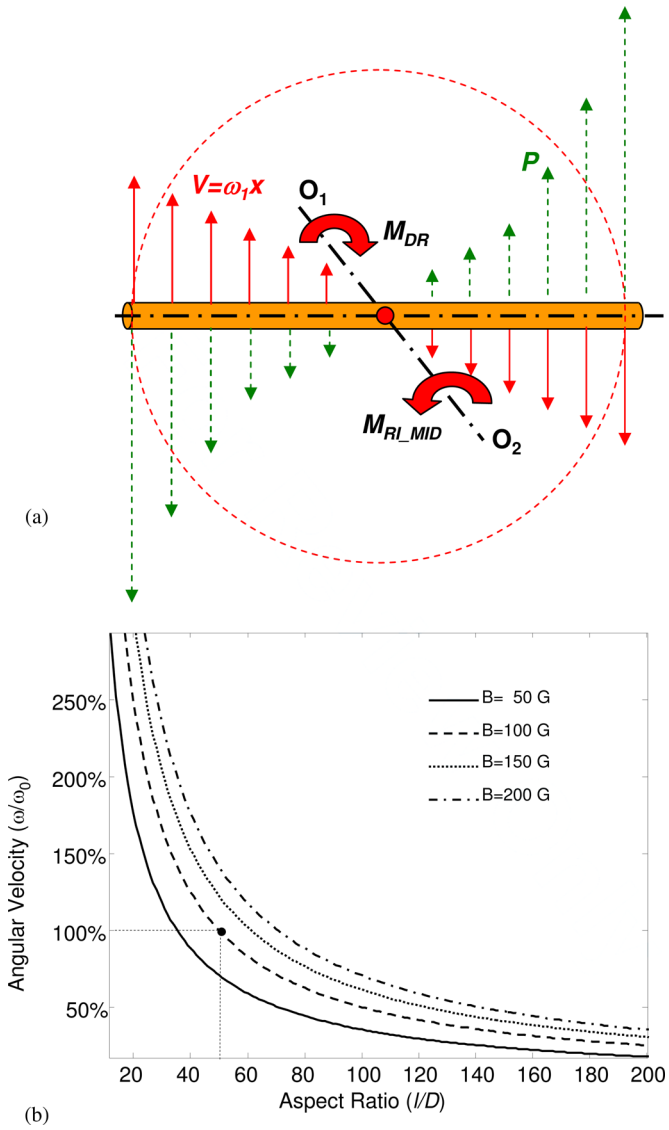

Fig. 3. Rotational maneuver of a floating nanowire with the diameter of 200 nm. (a) Nanowire rotates around its midpoint, governed by the driving magnetic toque and the fluidic drag force. The solid lines denote the distribution of velocity along the nanowire. The dashed lines denote the distribution of hydraulic resistance along the nanowire. (b) Angular velocity at equilibrium can be derived, showing that a longer nanowire has slower response to the external driving field than a shorter nanowire because of the larger fluidic drag force. The reference angular rotational velocity ω_0 is set for a 10-μm-long nanowire (200 nm in diameter, aspect ratio 50) under the field of 100 G. When the length increases to 20 μm (aspect ratio 100), the angular velocity decreases to 35.4% of the reference value. The angular velocity increases with increasing magnetic field. The external magnetic fields of the curves from left to right are 50, 100, 150, and 200 G, respectively.

toque in (1) [see Fig. 3(b)]. The angular velocity was represented by comparing with a reference angular velocity ω_0, which denotes the angular velocity of a 10-μm-long nanowire (200 nm in diameter, aspect ratio 50) under the field of 100 G. For analysis simplicity, this figure and the followings are all plotted at $\theta = 90°$. The angular velocity at smaller angles can be derived by multiplying the plotted values with a factor of sin θ. It is seen that under the same driving field and the same intersection angle, the angular velocity decreases with the increasing aspect ratio (length to diameter) of nanowires. For example, when the length of a nanowire (200 nm in diameter) increases from 10 μm to 20 μm, the angular velocity drops 64.6%. In other words, it takes longer for a more slender nanowire to reach equilibrium because of the larger drag force. Since the floating nanowire does not have an anchoring point contacting with the bottom surface, no obvious lateral movement is expected.

After the nanowire continues to fall and eventually settles to the bottom surface of the petri dish, the rotation of the nanowire follows a different route. Since the contact provides an anchoring point on the bottom surface, the nanowire rotates around this endpoint [see Fig. 4(a)]. The fluidic drag resistance torque becomes

$$M_{\mathrm{RI\_END}} = \int_0^l \frac{\omega_2^2 x^2 \rho}{2} D x \, dx = \frac{\omega_2^2 \rho D l^4}{8}. \tag{3}$$

Similar to the analysis in floating nanowires, the angular velocity ω_2 can be found by equaling the driving magnetic torque (M_{DR}) in (1) with the resistance torque ($M_{\mathrm{RI\_END}}$) in (3) [see Fig. 4(b)]. The angular velocity follows the same trend as in the floating case, but the magnitude reduces dramatically because of the larger fluidic resistance. In this case, we assume that the contacting endpoint of nanowire does not slip over the surface. During the rotation, the two endpoints of a nanowire alternatively serve as the anchoring point. As the result, large lateral displacement is expected as the rotation proceeds [see Fig. 4(c)]. It is easily derived that the lateral displacement during one rotation cycle is two times of the length of the nanowire. A nanowire can thus be manipulated to any arbitrary position on the lateral plane using the rotating external magnetic field.

E. Rotational Maneuver of a Cell–Nanowire Couple

The rotational maneuver of a cell–nanowire couple was studied. For analysis simplicity, it is assumed that a spherical cell contacts tangentially with a nanowire at its midpoint [see Fig. 5(a)]. The mechanical interaction between the cell and the nanowire does not induce substantial deformation of the cell body during rotation. Given the fact that the diameter of the cell is often on the order of a few micrometers, its surface area is much larger than that of the nanowire, it is plausible that the fluidic drag force of the cell–nanowire couple during rotation is mainly due to the fluidic resistance acting on the attached cell. For a floating cell–nanowire couple, the fluidic resistance torque can be determined as

$$M_{\mathrm{RI\_CPL}} = \int_{-R}^{R} \frac{\omega_3^2 x^2 \rho}{2} \sqrt{R^2 - x^2}\, x \, dx \tag{4}$$

where R denotes the radius of the cell. The angular velocity of the cell–nanowire couple (ω_3) at equilibrium was obtained using Mathematica software bundle. Fig. 5(b) shows that with a given driving torque, the angular velocity positively relates to the aspect ratio of the nanowire, i.e., greater the aspect ratio, faster the nanowire rotates. When the aspect ratio decreases to about 1, a 1-D nanowire reduces to a 0-D nanoparticle. The reduced magnetic dipole moment precludes efficient rotation of the

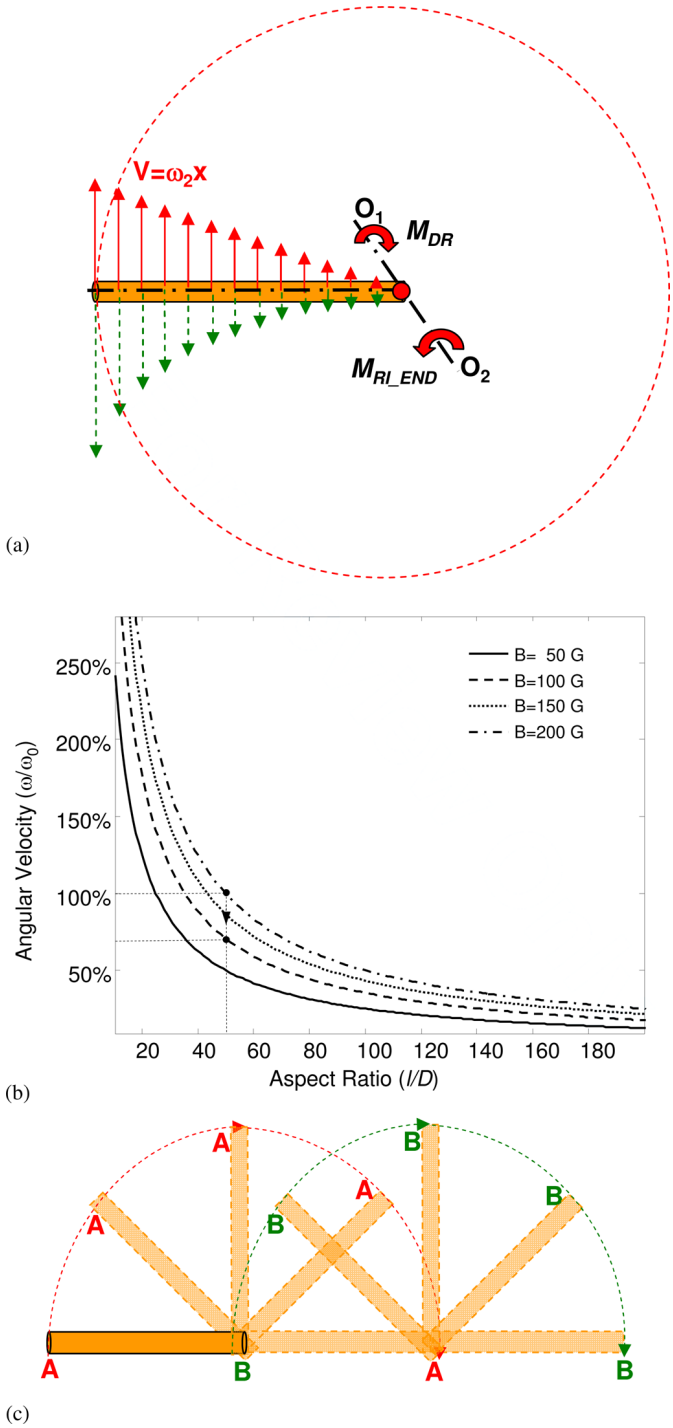

Fig. 4. Rotational maneuver of a nanowire that has established contacts with the bottom surface. The diameter of the nanowire is 200 nm. (a) Nanowire rotates around its endpoint. The solid lines denote the distribution of the velocity along the nanowire. The dashed lines denote the distribution of hydraulic resistance along the nanowire. (b) Angular velocity is a function of the aspect ratio and the external field. For comparison, the same reference, as in Fig. 3, is used. It is seen that when the nanowire rotates around its endpoint, the angular velocity decreases. For a 10-μm-long nanowire under 100 G, the angular velocity decreases to 71% of the reference value. The external magnetic fields of the curves from left to right are 50, 100, 150, and 200 G, respectively. (c) Two endpoints of the nanowire alternately contact with the bottom surface during the rotation, leading to a lateral displacement.

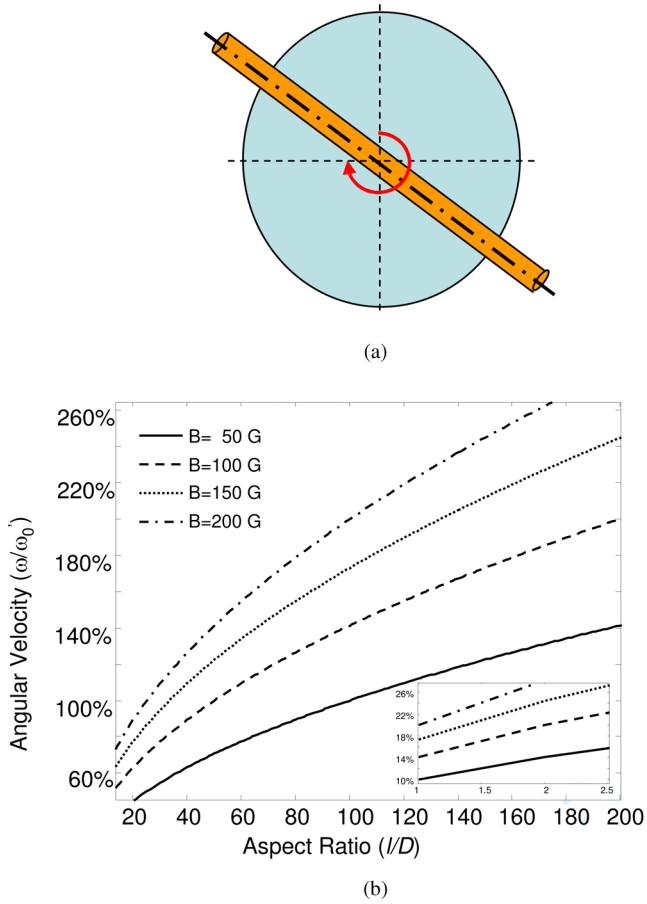

Fig. 5. Rotational maneuver of a floating cell–nanowire couple. The diameter of the nanowire is 200 nm. The spherical cell body has a diameter of 10 μm. (a) It is assumed that the midpoint of the nanowire coincides with the center of the cells. (b) Fluidic drag force is primarily due to the cell body. The angular velocity increases with the aspect ratio of the nanowire and the external field. The reference angular velocity ω_0 is set for a 10-μm-long nanowire (200 nm in diameter, aspect ratio 50) under the field of 100 G. The subfigure shows if the aspect ratio decreases to 1 (reduced to a nanoparticle), the angular velocity is only 14% of the reference value. The external magnetic fields of the curves from right to left are 50, 100, 150, and 200 G, respectively.

cell–nanowire couple, indicating that the spherical nanoparticles do not rotate the cells efficiently as nanowires do. Similar as floating nanowires, a floating cell–nanowire couple does not exhibit substantial lateral displacement under a rotating magnetic field due to the lack of anchoring points on the bottom surface.

III. Experimental Results

A. Manipulation of Nanowires

Fig. 6 shows the experiment results of nanowires rotation under the previous two suspension conditions (i.e., floating in the medium and contacting with the bottom surface). The medium containing nanowires was added to a 100-mm petri dish and shaken gently. Optical observation was performed shortly after the shaking to diminish the influence of the fluidic disturbance. The focal plane was carefully tuned to the horizontal plane

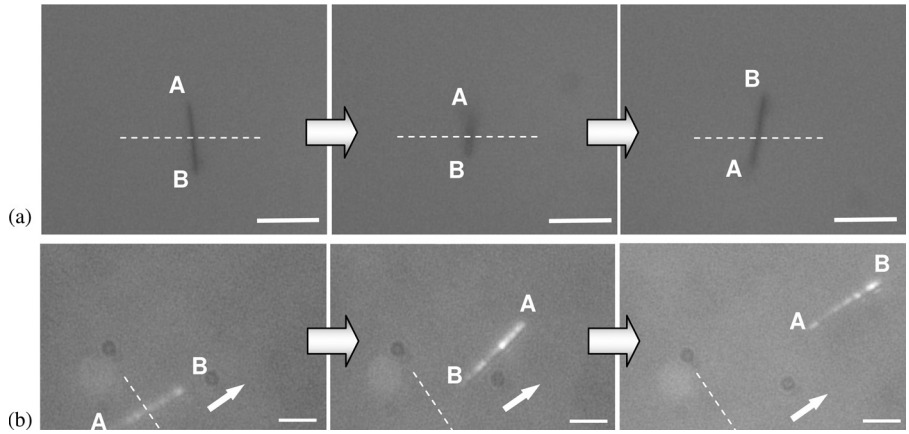

Fig. 6. Experimental validation of the nanowire rotation under two different suspending conditions. (a) Floating nanowire rotating around its midpoint did not exhibit substantial lateral displacement. (b) Nanowire contacting with the bottom surface had a lateral displacement under a rotating field. The spacebars indicate 10 μm. The dashed lines denote the normal direction of the rotating magnetic field.

where the subject nanowires floated. The nanowire rotation was indicated by the change of the projected length [see Fig. 6(a)]. The results showed that the focus plane changed modestly during the observation. The floating nanowire did not exhibit substantial lateral displacement, as evidenced by the small lateral displacement with respect to the stationary reference line, which further confirmed the assumption that the lateral displacement by the pull force due to the field nonuniformity can be neglected.

Under the second suspension condition, the nanowire suspension was kept stationary in the petri dish for 10 min to allow the sedimentation. The focal plane was adjusted to the bottom surface. After the nanowires laid on the surfaces, the rotating external field was applied. The rotation of the nanowire around one endpoint was observed [see Fig. 6(b)]. During the rotation, the endpoint that contacted with the bottom surface did not exhibit obvious lateral displacement, which validated the nonslip assumption. As the rotation proceeded, the nanowire moved laterally on the surface. It took less than 5 s for a 20-μm-long nanowire to finish one cycle, where the lateral displacement was measured about 40 μm.

Optical observations were performed in 20+ nanowires under each of the previous two suspension conditions. Control experiments were also performed with the same numbers of nanowires and with no magnetic field present in the surrounding regions. The nanowire rotation was recorded at 10 fps. The rotation angle of individual nanowires was derived from the ratio of the projection length to the full length of each nanowire (under 50$\times$ objective). Considering the measurement error, the angle variation among all the nanowires under a same field is within 5°. The angle variation does not change with the rotating angle. In the control group with no magnetic field, there was neither discernible rotation nor lateral movement during the entire observation.

B. Manipulation of Cell–Nanowire Couples

The manipulation of cell–nanowire couples was investigated. When a cell–nanowire couple settles to the bottom surface, its rotational maneuver under the rotating magnetic field varies with the length of the attached nanowire. If the nanowire is shorter than the diameter of the cell, the cell is rolling over the bottom surface while contacting all the time with the surface. Assuming there is nonslip condition between the cell and the bottom surface of the petri dish, the cell–nanowire movement is a combination of the translational motion within the lateral plane and the rotation around the midpoint of the nanowire (the center of the cell).

When the length of the nanowire is greater than the diameter of the cell, the rotational maneuver becomes a little more complicated since the endpoints of the nanowire contact two times with the bottom surface during each rotation cycle, as shown in Fig. 7(a). The process can be separated into two phases. In the first phase, the cell–nanowire couple rotates around the midpoint of the nanowire until one endpoint of the wire touches the bottom surface. In the second phase, the cell–nanowire couple rotates around the contacting endpoint, lifting the cell slightly off the surface until the cell contacts with the bottom surface again by the other side. The rotation proceeds as these two phases alternate, moving the cell–nanowire couple on the lateral surface. Fig. 7(b) shows the motion of a cell–nanowire couple under a rotating magnetic field. For such a cell–nanowire couple, the lateral displacement of over 1mm was achieved within 5 min using a modest magnetic field ranging from 50 to 200 G. The rotating rate was about 20 r/min. Faster motion is possible by increasing the rotating rate of the external field. The manipulation efficiency of the rotating magnetic field was evaluated by comparing the results to a reference traveling velocity under a stationary magnetic field of the same strength (200 G). The results showed that the lateral displacements of the nanowires under a rotating external field are much greater than that driven by the stationary field within the same time period.

According to Fig. 5(b), one can increase the lateral traveling velocity by using a longer nanowire. Nonetheless, it was observed in the experiments that a too long nanowire (over 30 μm) is not as efficient in rotating the cell–nanowire couple as compared to the slightly shorter ones. If the nanowire has a length much greater than the diameter of a cell, the couple may not follow the external field to rotate after one endpoint of the long nanowire contacts with the bottom surface. This may

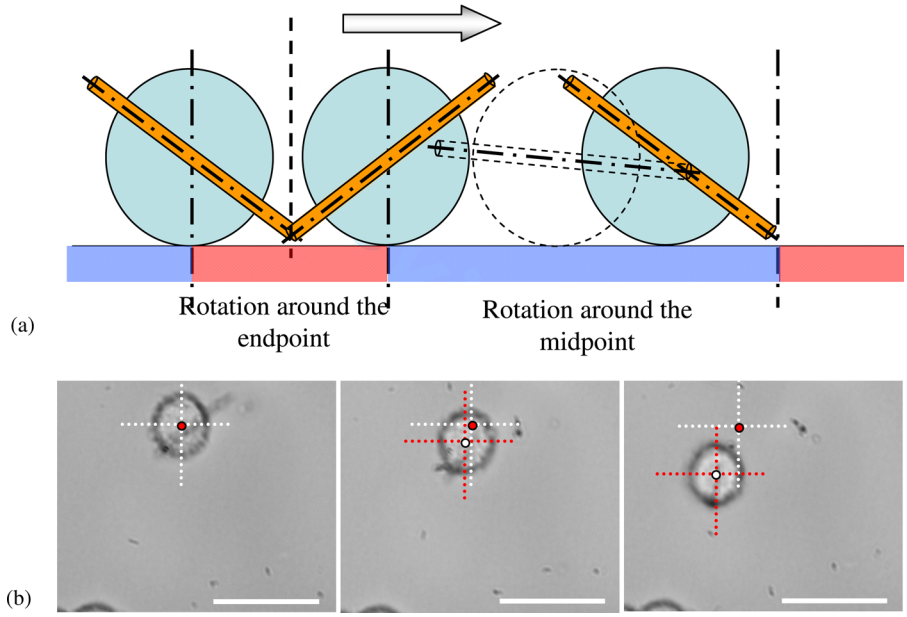

Fig. 7. Rotational maneuver of a cell–nanowire couple contacting with the bottom surface. (a) Rotation consists of two phases: 1) the rotation around the midpoint plus the lateral movement and 2) the rotation around the endpoint that lifts the cell out of the lateral surface. (b) Experimental observation of cell manipulation on the lateral surface under a rotating magnetic field. The spacebars indicate 20 μm.

be due to the large fluidic resistance acting on the cell that attached to the long nanowire. The experiments showed that the maximum lateral traveling velocity can be achieved when a cell was attached to a nanowire with the length close to the diameter of the cell, i.e., 10-μm-long nanowire for a cell with 10 μm in diameter. This finding is in consistence with previous research of the optimal cell separation efficiency [13].

C. Nanowire Clustering and 3-D Cell–Nanowire Assembly

Tissue engineering has attracted extraordinary attentions since it assembles cells into clusters with desired spatial arrangements by providing 2-D or 3-D scaffolds. With the *in vivo*-like spatial arrangements, these multicellular assemblies may be used as an *in vitro* model for studying cellular behaviors under various controllable conditions [20], [21]. More important, the assembled structures hold the promise of being transplanted into organisms for tissue repair and replacement [22]–[25]. It is known that the ferromagnetic nanowires are able to attract and connect with each other when they are brought approached due to the interaction of their magnetic dipoles. Such connection has shown effectiveness in assembling 1-D cell chains [17]. Here, we explore the use of the rotational maneuver of ferromagnetic nanowires for creating 3-D assemblies. Given the fact that the rotating external magnetic field lifts the subject nanowires out of the lateral plane, these nanowires are expected to connect with each other and form 3-D structures. The beauty of this study is to assemble the cells into desired spatial arrangement without the help of predefined scaffolds. The work will also allow 3-D multicellular assemblies to be formed in the time-effective fashion by precluding cellular adaptation to local environments.

First, the assembly of individual nanowires was demonstrated. Nanowires with the length of about 20 μm were added to the medium and allowed to settle to the bottom surface. The external magnetic field was applied to manipulate the nanowires. As a nanowire rotated, it picked up other nanowires on its way due to the magnetostatic interaction between their dipoles and formed a cluster. Upon connection of the nanowires, a new magnetic dipole formed within the assembled cluster. As a result, the cluster had greater spatial dimensions than individual nanowires, and thus, a greater dipole moment. Therefore, the cluster has a larger lateral displacement than individual nanowires during the same period of time. Experiments showed that during rotation the nanowire cluster kept a rod shape. The longitudinal axis is normal to the direction of the lateral motion. Such geometry minimizes the fluidic resistance and allows large traveling velocity. To demonstrate cluster manipulation along a predetermined route [see Fig. 8(a)], a permanent magnet positioned 90° with the previous one [as shown in Fig. 2(a)] was used to induce lateral motion along the perpendicular direction. The two permanent magnets were used alternatively to drive the cluster to desired locations. During the process, the nanowire cluster "*cleaned*" its way by picking up individual nanowires on the bottom surface [see Fig. 8(b)]. The results showed that it took less than 1 min to pick up over 95% nanowires within an area of 10^4 μm^2.

Multicellular assemblies were also demonstrated. Fig. 9(a) shows the manipulation of a cell–nanowire couple to approach another couple under the rotating magnetic field. The multiple-couple cluster was formed as the attached nanowires connect with each other. No detachment was observed in the subsequent rotation. By continuing the process, the cluster served as a seed for picking up other cell–nanowire couples on the surface and forming a large rod-shaped cell–nanowire assembly [see Fig. 9(b)–(d)]. The assembly can be wrapped by rotating the field along the longitudinal axis of the rod-shaped cluster to form a more spherical geometry. Optical examination showed

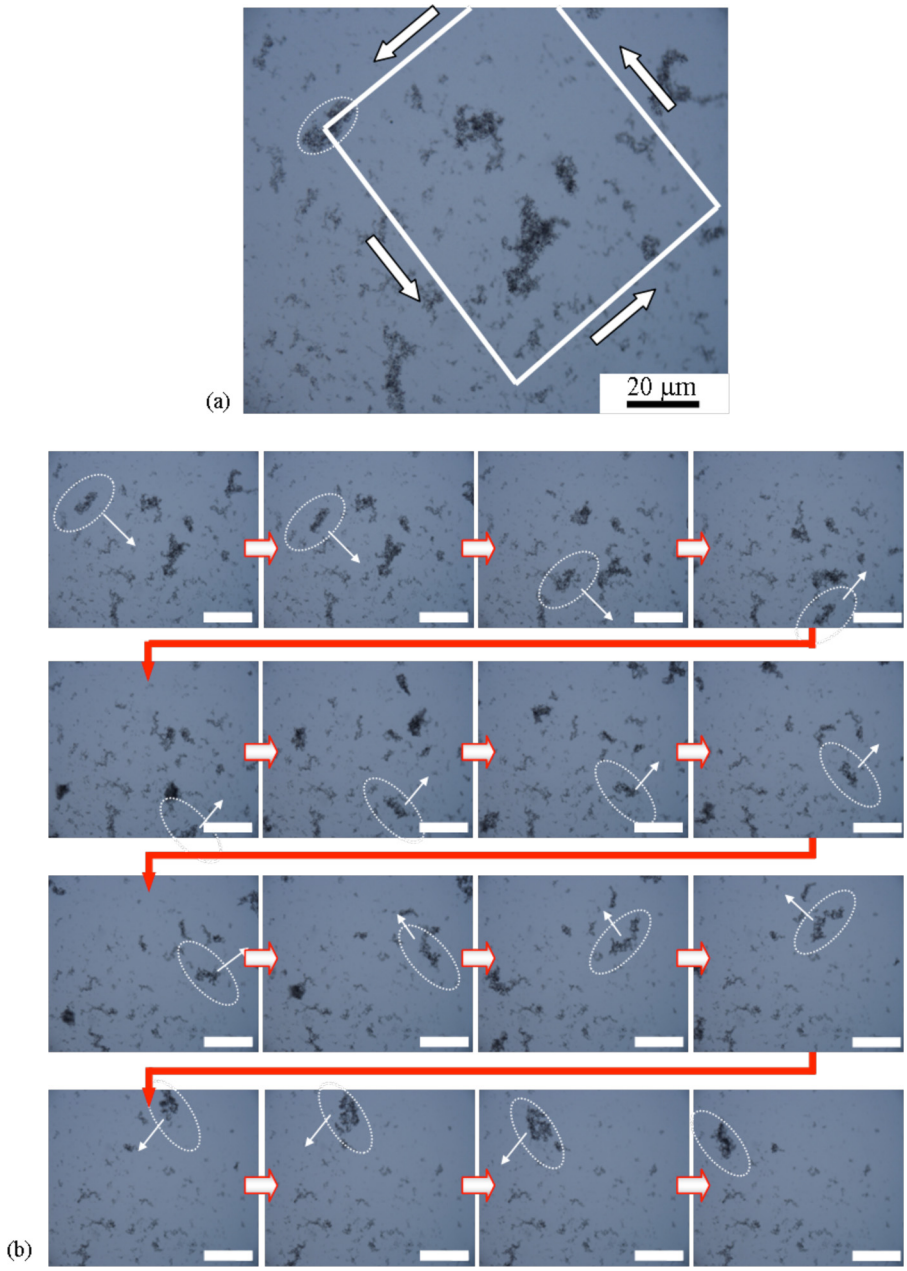

Fig. 8. Nanowire clustering process under a rotating external field. (a) Predefined route of the manipulation. (b) Time lapse pictures show the manipulation process. The spacebars in (b) indicate 30 μm.

that the cluster holds the cells in a 3-D fashion. The thickness of a representative rod-shaped cluster is over 200 μm. The lateral dimension is over 1 mm. The size and the geometry of the cluster can be adjusted by controlling the traveling route of the seed cluster for selective picking up and wrapping.

IV. Discussion

A. Cell Proliferation and Nanowire Internalization

Timing is a critical factor for efficient cell manipulation using the rotational maneuver of nanowires. The manipulation needs to be performed right after the cells settle to the bottom surface. If the cells are left on the surface for long, they may start to develop adhesion with the bottom surface and spread. Experiments showed that after the cells had been allowed to attach for about 1 h, about 80% of the cells adhered to the bottom surface and did not respond to the external field, indicating that the magnetic torque generated by a modest external field (on the order of 100 G) was not able to compete with the increasing cellular adhesive force. After the cells were cultured for 24 h, most cells lost their spherical geometry. The attached nanowires were found being internalized by the cells, similar as previously reported [7]. It may due to the fact that the nickel is an essential structural component of the metalloprotein and can fuse with lysosomes [26]. The image taken after 24 h continuous culturing in the growth medium from the point of cell seeding is

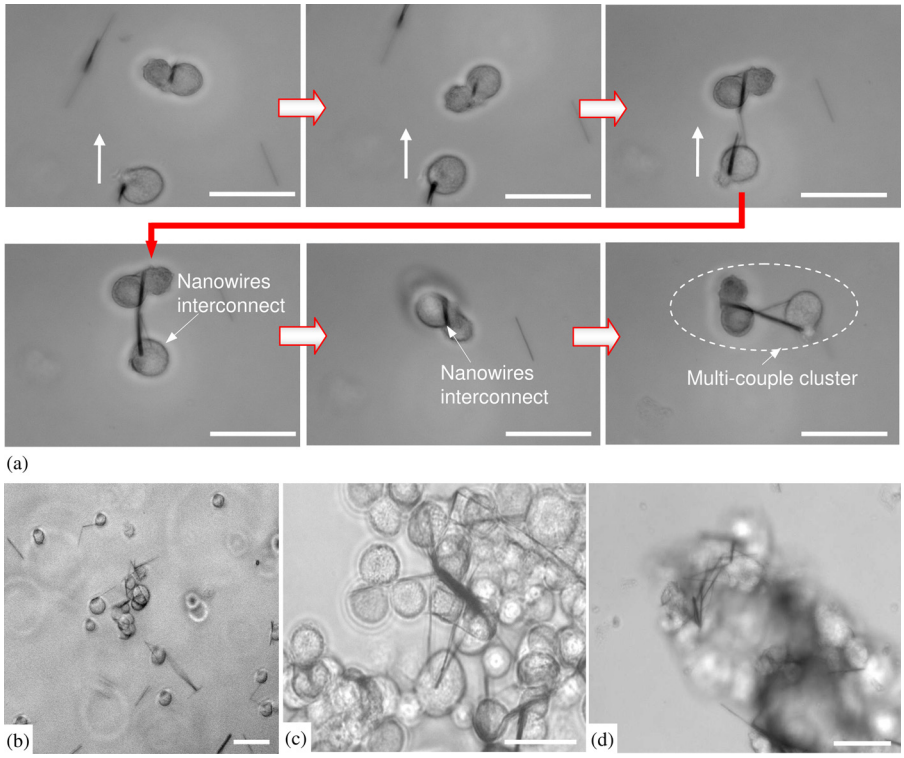

Fig. 9. Multicellular clustering using the rotational maneuver. (a) Cell–nanowire couple was brought approached to other couples to assemble a large cluster upon nanowires connection. (b)–(d) 3-D cell–nanowire clusters were formed by picking up all the cell–nanowire couples on the lateral surface. The spacebars indicate 20 μm.

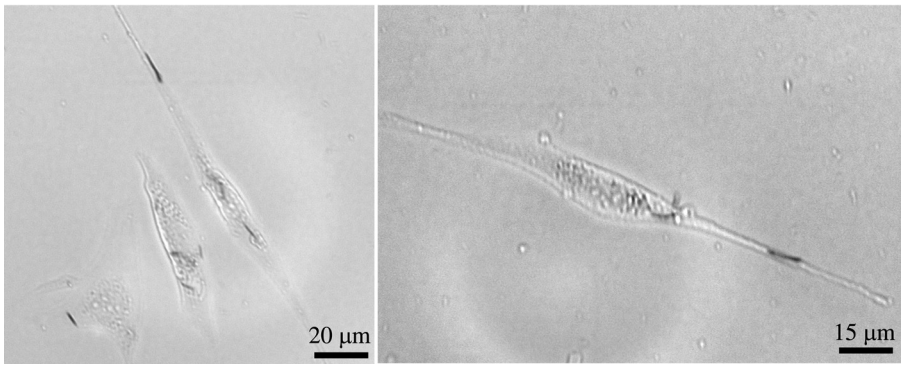

Fig. 10. Nanowire internalization by the skeletal myoblasts shows that the nanowires, if internalized, may affect the cell morphology. The image was taken after 24 h continuous culturing in growth medium from the point of cell seeding.

shown in Fig. 10. This experiment indicated that the nanowires may, to some extent, affect the spreading profile of the adherent cells, i.e., the cells extend the pseudopodia along the longitudinal axis of the nanowires. This is explained by the influence of nanowires on cytoskeleton rearrangement. The in-depth study of the influence of internalized nanowires on cell morphology is currently underway.

B. Biocompatibility of Nanowires

The viability of the skeletal myoblasts is not significantly compromised by the attached nanowires. The cytotoxicity of nickel has been discussed in previous studies [7], [16], [26]. Here, the cell viability was assessed by culturing the cells for 24 h after they had been attached with the nickel nanowires. The results showed that 85% cells attached with nanowires were able to adhere on the bottom surface and spread. After the nonadhered cell–nanowire couples were aspirated, the adherent cells continued to proliferate and reached confluence after about 72 h. There was not obvious cell detachment during cell proliferation.

Despite of the promising potential of ferromagnetic nanoparticles and nanowires for cell manipulation and analysis, one critique of these nanomaterials is that they are not readily degradable by the metabolism of biological systems, and may coexist with the cells for a fairly long period of time. The potential adverse effects of metallic nanowires on cell behavior can be reduced as the proliferation proceeds because the volume ratio of nanomaterials to the cells continues to decrease. To

further reduce the adverse effects of these metallic nanomaterials, nanowires can be encapsulated within a more biocompatible polymer material [27], [28]. This avoids direct contact of metallic nanomaterials with cells while retaining the manipulability of these nanomaterials by external magnetic fields. One can also fabricate 1-D nanomaterials using biodegradable nanomaterials with ferromagnetic or paramagnetic properties for cell manipulation [29].

C. Control of Cell–Nanowire Couples and Clusters

Efficient manipulation of cell–nanowire couples is compromised by several factors. First, the midpoint of the nanowire is not always at the center of the cell. This may change the rotation center of the cell–nanowire couples, and lead to an increased resistance toque. Second, during the formation of cell–nanowire clusters, the external rotating field rotates all the cell–nanowire couples, making it difficult to selectively manipulate a single couple. A practical solution is to use a large cell–nanowire couple as the seed. The higher lateral traveling velocity will allow the seed to catch up smaller couples during the rotation, and to enlarge the cluster.

The manipulation process is also affected by the magnetostatic interactions between the nanowires attached on cell–nanowire clusters. The analysis of a simple system composed of few ferromagnetic nanowires is actually much more intricate than it appear to be [30]. The arbitrary distribution of nanowires in the clusters further complicates the analytical process. Fortunately, although the previous factors have not been fully taken into account, experiments show that the analysis of a cell–nanowire couple in (4) provides a good start point to understand the essence of the rotational maneuver of the cell–nanowire couple. More precise geometric control of the clusters made of multiple cell–nanowire couples will be studied in the future.

V. Conclusion

This study explores the use of the rotational maneuver of nanowires for cell manipulation and clustering under an external magnetic field. The out-of-plane rotation of the nanowire with larger magnetic dipole moments allows efficient manipulation of the attached cells. The rotational maneuver and manipulation efficiency are interpreted by investigating two different suspension conditions. The movement of 3-D nanowire clusters and cell–nanowire clusters was experimentally validated. Several factors that involved in the complex formation process of 3-D clusters are discussed. The results obtained in this study show that the rotational maneuver of nanowires are advantageous over previous nanowire-based manipulation technologies by avoiding the fabrication of local magnetic or metallic components and allowing rapid lateral displacement using a modest external magnetic field. It thus facilitates the integration of magnetic nanomaterials into cellular objects. This study is expected to open new prospective for pattern-less cell manipulation, and help the scaffoldless fabrication of 3-D cell assemblies in various tissue engineering studies.

Acknowledgment

The authors would thank Dr. S. Agarwal at Oral Biology for her generous supply of C2C12 skeletal myoblasts. The authors would also thank the undergraduate researcher J. Ebel for his assistance.

References

[1] R. Giordano, L. Lazzari, and P. Rebulla, "Clinical grade cell manipulation," *Vox Sang*, vol. 87, pp. 65–72, Aug. 2004.

[2] C. Yi, C. Li, S. Ji, and M. Yang, "Microfluidics technology for manipulation and analysis of biological cells," *Anal. Chim. Acta*, vol. 560, pp. 1–23, 2006.

[3] J. Voldman, R. A. Braff, M. Toner, M. L. Gray, and M. A. Schmidt, "Holding forces of single-particle dielectrophoretic traps," *Biophys. J.*, vol. 80, pp. 531–541, Jan. 2001.

[4] J. Voldman, "Dielectrophoretic Traps for Cell Manipulation," in *BioMEMS and Biomedical Nanotechnology*. New York: Springer-Verlag, 2007, pp. 159–186.

[5] M. Ozkan, M. Wang, C. Ozkan, R. Flynn, and S. Esener, "Optical manipulation of objects and biological cells in microfluidic devices," *Biomed. Microdevices*, vol. 5, pp. 61–67, 2003.

[6] M. Zahn, "Magnetic fluid and nanoparticle applications to nanotechnology," *J. Nanopart. Res.*, vol. 3, pp. 73–78, 2001.

[7] A. Prina-Mello, Z. Diao, and J. M. Coey. (2006, Sep. 5). Internalization of ferromagnetic nanowires by different living cells, *J. Nanobiotechnol.* [Online]. *4*, p. 9, Available: http://www.pubmedcentral.nih.gov/articlerender.fcgi?tool=pubmed&pubmedid=16953891

[8] T. Yoshino, H. Hirabe, M. Takahashi, M. Kuhara, H. Takeyama, and T. Matsunaga, "Magnetic cell separation using nano-sized bacterial magnetic particles with reconstructed magnetosome membrane," *Biotechnol. Bioeng.*, vol. 101, no. 3, pp. 470–477, Mar. 25, 2008.

[9] J. Kandzia, M. J. Anderson, and W. Muller-Ruchholtz, "Cell separation by antibody-coupled magnetic microspheres and their application in conjunction with monoclonal HLA-antibodies," *J. Cancer Res. Clin. Oncol.*, vol. 101, pp. 165–170, 1981.

[10] L. Fracioso, A. M. Taurino, A. Forleo, and P. Siciliano, "nanowires array fabrication and gas sensing properties," *Sens. Actuators B: Chem.*, vol. 130, pp. 70–76, 2008.

[11] S. Chikazumi and C. D. Graham, *Physics of Ferromagnetism*, 2nd ed. New York: Oxford Univ. Press, 1997.

[12] D. Whang, S. Jin, Y. Wu, and C. M. Lieber, "Large-scale hierarchical organization of nanowire arrays for integrated nanosystems," *Nano Lett.*, vol. 3, pp. 1255–1259, 2003.

[13] A. Hultgren, M. Tanase, C. S. Chen, and D. H. Reich, "High-yield cell separations using magnetic nanowires," *IEEE Trans. Magn.*, vol. 40, no. 4, pp. 2988–2990, Jul. 2004.

[14] N. J. Sniadecki, R. A. Desai, S. A. Ruiz, and C. S. Chen, "Nanotechnology for cell-substrate interactions," *Ann. Biomed. Eng.*, vol. 34, pp. 59–74, Jan. 2006.

[15] M. A. Lan, C. A. Gersbach, K. E. Michael, B. G. Keselowsky, and A. J. Garcia, "Myoblast proliferation and differentiation on fibronectin-coated self assembled monolayers presenting different surface chemistries," *Biomaterials*, vol. 26, pp. 4523–4531, Aug. 2005.

[16] A. Hultgren, M. Tanase, C. S. Chen, G. J. Meyer, and D. H. Reich, "Cell manipulation using magnetic nanowires," *J. Appl. Phys.*, vol. 93, pp. 7554–7556, 2003.

[17] M. Tanase, E. J. Felton, D. S. Gray, A. Hultgren, C. S. Chen, and D. H. Reich, "Assembly of multicellular constructs and microarrays of cells using magnetic nanowires," *Lab Chip*, vol. 5, pp. 598–605, Jun. 2005.

[18] K. Ino, A. Ito, and H. Honda, "Cell patterning using magnetite nanoparticles and magnetic force," *Biotechnol. Bioeng.*, vol. 97, pp. 1309–1317.

[19] K. Ino, M. Okochi, N. Konishi, M. Nakatochi, R. Imai, M. Shikida, A. Ito, and H. Honda, "Cell culture arrays using magnetic force-based cell patterning for dynamic single cell analysis," *Lab Chip*, vol. 8, pp. 134–142, Jan. 2008.

[20] M. Halbach, F. Pillekamp, K. Brockmeier, J. Hescheler, J. Muller-Ehmsen, and M. Reppel, "Ventricular slices of adult mouse hearts—A new multicellular *in vitro* model for electrophysiological studies," *Cell Physiol. Biochem.*, vol. 18, pp. 1–8, 2006.

[21] G. Hamilton, "Multicellular spheroids as an in vitro tumor model," *Cancer Lett.*, vol. 131, pp. 29–34, Sep. 11, 1998.

[22] D. W. Hutmacher, "Scaffold design and fabrication technologies for engineering tissues—State of the art and future perspectives," *J. Biomater. Sci. Polym. Ed.*, vol. 12, pp. 107–124, 2001.
[23] J. P. Vacanti, "Tissue engineering: from bench to bedside via commercialization," *Surgery*, vol. 143, pp. 181–183, Feb. 2008.
[24] W. Yan, S. George, U. Fotadar, N. Tyhovych, A. Kamer, M. J. Yost, R. L. Price, C. R. Haggart, J. W. Holmes, and L. Terracio, "Tissue engineering of skeletal muscle," *Tissue Eng.*, vol. 13, pp. 2781–2790, Nov. 2007.
[25] K. Jakab, C. Norotte, B. Damon, F. Marga, A. Neagu, C. L. Besch-Williford, A. Kachurin, K. H. Church, H. Park, V. Mironov, R. Markwald, G. Vunjak-Novakovic, and G. Forgacs, "Tissue engineering by self-assembly of cells printed into topologically defined structures," *Tissue Eng. Part A*, vol. 14, pp. 413–421, Mar. 2008.
[26] K. S. Kasprzak, F. W. Sunderman, Jr., and K. Salnikow, "Nickel carcinogenesis," *Mutat. Res.*, vol. 533, pp. 67–97, Dec. 10, 2003.
[27] R. Gunawidjaja, C. Jiang, S. Peleshanko, M. Ornatska, S. Singamaneni, and V. V. Tsukruk, "Flexible and robust 2D arrays of silver nanowires encapsulated within freestanding layer-by-layer films," *Adv. Funct. Mater.*, vol. 16, pp. 2024–2034, 2006.
[28] H. Q. Cao, Z. Xu, H. Sang, D. Sheng, and C. Y. Tie, "Template synthesis and magnetic behavior of an array of cobalt nanowires encapsulated in polyaniline nanotubules," *Adv. Mater.*, vol. 13, pp. 121–123, 2001.
[29] S. T. Tan, J. H. Wendorff, C. Pietzonka, Z. H. Jia, and G. Q. Wang, "Biocompatible and biodegradable polymer nanofibers displaying superparamagnetic properties," *Chemphyschem*, vol. 6, pp. 1461–1465, Aug. 12, 2005.
[30] J. Velázquez, C. García, M. Vázquez, and A. Hernando, "Interacting amorphous ferromagnetic wires: A complex system," *J. Appl. Phys.*, vol. 85, pp. 2768–2774, 1999.

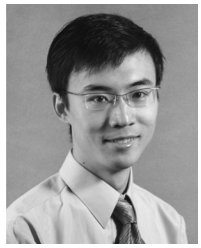

Yi Zhao (M'06) received the B.S. and M.S. degree in mechanical engineering from Tsinghua University, Beijing, China in 2000 and 2002, respectively, and the Ph.D. degree in manufacturing engineering from Boston University, Boston, MA, in 2006.

He is currently an Assistant Professor of biomedical engineering at the Ohio State University, Columbus, where he leads the Laboratory for BioMedical Microsystems. His current research interests include studies of microelectromechanical/nanoelectromechanical devices for biomedical and clinical applications, including investigation of novel materials, design and fabrication technologies, as well as the interface with living organisms at multiple scales. He is the author or coauthor of more than 50 publications in biomedical and nanotechnology.

Hansong Zeng received the B.S. and M.S. degrees in thermal engineering from Xi'an Jiaotong University, Xi'an, China, in 2004 and 2007, respectively. He is currently working toward the Ph.D. degree in the Laboratory for Biomedical Microsystems, Department of Biomedical Engineering, the Ohio State University, Columbus, OH.

His current research interests include the design and fabrication of microfludic-based BioMEMS, and their applications in biomedical research and clinical diagnosis.